Journal of Alloys and Compounds 698 (2017) 555–564

Contents lists available at ScienceDirect

Journal of Alloys and Compounds

journal homepage: http://www.elsevier.com/locate/jalcom

Influence of Al doping on the structural, morphological, optical, and gas sensing properties of ZnO nanorods

R. Sankar ganesh [a, b], M. Navaneethan [c], Ganesh Kumar Mani [d], S. Ponnusamy [b, *], K. Tsuchiya [d], C. Muthamizhchelvan [b], S. Kawasaki [e], Y. Hayakawa [a, c, **]

[a] Graduate School of Science and Technology, Shizuoka University, 3-5-1 Johoku, Naka-ku, Hamamatsu, Shizuoka 432-8011, Japan
[b] Department of Physics and Nanotechnology, SRM University, Kattankulathur, Kancheepuram 603203, Tamil Nadu, India
[c] Research Institute of Electronics, Shizuoka University, 3-5-1 Johoku, Naka-ku, Hamamatsu, Shizuoka 432-8011, Japan
[d] Department of Precision Engineering, Micro/Nano Technology Center, Tokai University, Shonan Campus Hiratsuka, Kanagawa 259-1292, Japan
[e] Department of Materials Science and Engineering, Nagoya Institute of Technology, Gokiso-ku, Showa-ku, Nagoya 466-8555, Japan

ARTICLE INFO

Article history:
Received 5 November 2016
Received in revised form
13 December 2016
Accepted 15 December 2016
Available online 18 December 2016

Keywords:
Ammonia
ZnO
Al doping
Gas sensor
Nanostructured materials

ABSTRACT

Ammonia is one of the most hazardous substance and highly toxic to human health when inhaled above the moderate level. Sensing ammonia is one most challenging task at low temperature level and room temperature. ZnO and Al-doped ZnO nanostructures were successfully synthesized by sol–gel method, and their structural, optical, morphological, and gas sensing properties were investigated. Field-emission scanning electron microscopy revealed that the ZnO nanorods transformed into particles upon incorporation of Al. Transmission electron microscopy and high-resolution transmission electron microscopy confirmed that both the ZnO nanorods and Al-doped ZnO nanoparticles were crystalline. Fourier transform infrared spectroscopy analysis indicated the presence of Zn–O and Al–O in the nanostructures. Energy-dispersive X-ray spectroscopy revealed the presence of Al in the Al-doped ZnO materials. The ammonia gas sensing analysis revealed that the Al-doped ZnO nanoparticles displayed a higher response than the ZnO nanorods. Moreover, among the doped samples, that containing 6 wt% Al dopant exhibited the highest response of 350 when exposed to 100 ppm ammonia gas. The higher sensing efficiency of the Al-doped ZnO nanostructures was attributed to changes in structural defects in Al-doped ZnO, as confirmed by X-ray photoelectron spectroscopy analysis.

1. Introduction

Metal oxide semiconductors have drawn much attention in gas sensing and play a vital role in safety control, disease diagnostic, controlling air quality, and detecting harmful and toxic gases [1–5]. Among the various semiconductor metal oxides, TiO_2 and ZnO are the most widely investigated semiconducting materials because of their attractive properties such as high carrier mobility, non-toxicity, excellent optical absorption, and high stability [6]. Furthermore, when compared with TiO_2, ZnO has higher electron mobility, longer electron lifetime, and greater intrinsic impurities, which can reduce the electrical resistance and increase electron transfer. ZnO possesses various defects such as oxygen vacancies, zinc interstitials, and oxygen interstitials which can enhance catalytic reactions in the gas sensor [7,8]. The popular sensing mechanism of metal oxide semiconductor gas sensors is based on the variation of electrical conductivity in the presence and absence of the test gas.

Metal oxide gas sensors with greater sensitivity and selectivity can be prepared by introducing dopants in the primary material structures. Specifically, dopants can enhance the gas sensing properties by changing the energy band structure and morphology of the semiconductor material, increasing the surface-to-volume ratio, and creating more centers for gas interaction on the metal oxide semiconductor surface [9–12]. As demonstrated in the literature, the sensitivity and conductivity of ZnO nanomaterials can be improved by Al doping. Al impurity plays a crucial role in accelerating chemical reactions in the gas sensor. Additionally, Al dopant can enhance the oxygen adsorption capacity, which can

---

* Corresponding author.
** Corresponding author. Department of Physics and Nanotechnology, SRM University, Kattankulathur, Kancheepuram 603203, Tamil Nadu, India.
E-mail addresses: suruponnus@gmail.com (S. Ponnusamy), royhaya@ipc.shizuoka.ac.jp (Y. Hayakawa).

http://dx.doi.org/10.1016/j.jallcom.2016.12.187

increase solid–gas interaction events. Moreover, Al^{3+} can effectively substitute Zn^{2+} in the crystal lattice owing to its smaller ionic radious ($r_{Al} = 0.054$ nm and $r_{Zn} = 0.074$ nm) [13,14]. Liu et al. [15] studied the optical and gas sensing properties of Al-doped ZnO, which were prepared by sol–gel, and examined the corresponding thin films as an ethanol sensing device. Vattappalam et al. [16] synthesized Al-doped ZnO thin films by successive ionic layer adsorption and reaction method and observed considerable reduction in resistance in the presence of ethanol vapor. Hence, the films can be used as fast-response sensors for ethanol vapors. Yoo et al. [17] showed that Al-doped ZnO exhibited a higher response when compared with pure ZnO in the detection of dimethyl methylphosphonate. Zhong et al. [18] reported the synthesis of Al-doped ZnO nanorods grown on a glass substrate and annealed under hydrogen atmosphere. Patil et al. [19] demonstrated the considerable greater sensitivity of Al-doped films to CO_2 gas over that of pure ZnO film. Several techniques can be used for preparing Al-doped ZnO thin films [20–22].

Ammonia is one of the most widely used materials in different industries such as chemical, petrochemical and various other manufacturing units of explosives, plastics, textiles, pesticides and dyes. Ammonia is one of the significant toxic gas having a threshold limit of 25 ppm, which damage the human respiratory system, eyes, skin and long term inhalation of ammonia leads to death [23]. So, it is very much essential to detect ammonia at room temperature in working environment. Sensing of ammonia gas by different nanostructures of metal oxide such as ZnO, SnO_2, In_2O_3 were investigated at different temperatures (100–300 °C). ZnO nanorods had shown maximum response of 80 and 18 for 800 ppm at 300 °C and 100 °C, respectively [24]. ZnO nanoparticle showed better ammonia sensing response of 260 and 19 for 800 p.m. at 300 °C and 100 °C, respectively [24]. To achieve better sensing of ammonia, ZnO nanostructured materials are inspired. On the other hand, ZnO nanostructured materials have the limitation of operating at lower temperature, making a great challenge to employ this in mobile application with durability. To overcome the limitation of low temperature operation of ZnO nanostructured materials, we have utilized Al-doped ZnO materials to enhance the ammonia sensing response at even low temperature in this research.

Among the different synthetic methods, the sol–gel process has distinct advantages over other approaches. For instance, it allows excellent material composition control and offers a simple method to synthesize nanoparticles. In the present work, we report a simple sol–gel method for preparing Al-doped ZnO. The prepared materials were characterized by X-ray diffraction, field-emission scanning electron microscopy, transmission electron microscopy, energy-dispersive X-ray spectroscopy, UV–visible spectroscopy, Fourier transform infrared spectroscopy, Raman spectroscopy and N_2 adsorption–desorption analysis. Subsequently, the gas sensing properties of the prepared materials towards ammonia gas were examined.

2. Materials and methods

2.1. Materials

Zinc acetate ($Zn(O_2CCH_3)_2(H_2O)$), aluminum nitrate, citric acid, and ammonia were purchased from Merck India. All other reagents and solvents were received and used without any further purification.

2.2. Preparation of undoped ZnO and Al-doped ZnO

Al-doped ZnO materials at varying Al dopant contents were prepared as follows. $Zn(O_2CCH_3)_2(H_2O)$ (1 M) and aluminum nitrate at varying weight percentage (0, 3, 6, 9, 12%) were dissolved in deionized water (50 mL) and stirred for 1 h at 80 °C. The pH of the solution was controlled with citric acid. The solution transformed into a gel upon addition of ammonia (10 mL). The gel was then cooled to room temperature and collected, centrifuged at 6000 rpm for 5 min, washed with deionized water and ethanol for several times, and dried at 100 °C in a hot air oven. The dried product was collected and calcined at 600 °C for 4 h.

2.3. Characterization of undoped ZnO and Al-doped ZnO

The crystalline structure of the prepared materials was determined by X-ray diffraction (XRD) on an X'pert PRO (PANalytical) advanced X-ray diffractometer using Cu Kα radiation ($\lambda = 1.5406$ Å) and a 2θ scanning range of 20–80° and a scanning rate of 0.025°/s. The microstructure of the products was observed by field-emission scanning electron microscopy (FESEM; QUANTA FEG) and transmission electron microscopy (TEM; JEOL JEM 2100F) operating at accelerating voltages of 15 and 200 kV, respectively. The components of the products were evaluated by energy-dispersive X-ray spectroscopy (EDX). Raman spectroscopy analysis was performed to evaluate structural disorder, and vibrational and defect modes in the prepared samples; the spectra were recorded on a JASCO NR 1800 Raman spectrometer equipped with a Nd:YAG laser. The optical properties of the products were measured using a PerkinElmer lambda 5 UV–visible spectrophotometer. Fourier transform infrared (FTIR) spectra were recorded by JASCO MFT 2000 using KBr pellet technique. Brunauer–Emmett–Teller (BET) specific surface areas were analyzed by Gemini2375, Shimadzu.

2.4. Ammonia gas sensing

To measure the sensing characteristics, the sensing elements are prepared by coating thick film of undoped ZnO and Al-doped ZnO (0, 3, 6, 9, 12%) on the substrates using mixture of ethyl cellulose and terpineol as binder. The sensing elements were subjected to heat treatment at 200 °C for 2 h to remove the organic elements. The silver paste coated over the sensing element as electrodes to take the electrical response. Various concentration of ammonia gas flowed through the sensing element and the response was calculated by $S = \frac{R_a}{R_g}$where R_a and R_g are the resistance of the sensing element in air and target gas, respectively.

3. Results and discussion

3.1. Structural and morphological analysis of undoped ZnO and Al-doped ZnO

The XRD patterns of the synthesized undoped ZnO and Al-doped ZnO (AZO) with different Al contents are depicted in Fig. 1. AZO exhibited a well-crystalline wurtzite ZnO crystal structure (JCPDS card no. 36-1451). All the samples of undoped and Al-doped ZnO featured diffraction peaks at 31.8°, 34.51°, 36.37°, 47.59°, 56.64°, 62.86°, 66.40°, 67.91°, 69.15°, 72.69°, and 76.95°, which corresponded to the (100), (002), (101), (102), (110), (103), (200), (112), (201), (004), and (202) planes of ZnO and AZO, respectively [25]. The peaks observed at approximately 2θ 31.21°, 36.8°, and 55.72° confirmed the presence of Al in the ZnO nanoparticles. The grain size of the ZnO and AZO nanoparticles was calculated using the Scherrer's formula, $D = \frac{K\lambda}{\beta \cos\theta}$, where K denotes the Scherrer's constant (0.89), D is the particle size, λ is the wavelength of the X-ray Cu Kα radiation (1.5406 Å), β is the full-width at half-maximum in radians of respective peaks, and θ is the Bragg's diffraction angle in degrees. As observed from Table 1, the average grain size of AZO decreased from 78 to 52 nm with increasing Al concentrations. As seen in the Table 1, doping of aluminum clearly reduces the crystallite size of samples (3 and 6%) because to the ionic radius of Al^{3+} (0.535 Å) is smaller than that of Zn^{2+} (0.74 Å) ion. The length of the c-axis is expected to be shorten, if the most of the Al atoms are substituted into Zn sites. In addition to that the covalent bond length of Al-O is shorter than Zn-O, which results in decrease of the unit cell. However further increase in concentration of Al-doping ratio (9 and 12%) in ZnO which induces the crystallite growth and the particle size increased. It may be due to exceeding the thermodynamic limit of solubility of Al in ZnO [26,27].

The morphology of the prepared ZnO and AZO materials was studied by FESEM (Fig. 2) and TEM (Figs. 3 and 4). As observed in Fig. 2a, ZnO featured a nanorod-like morphology; the nanorods were approximately 1.5 μm in length. In contrast, the AZO materials at low Al concentrations featured an irregular sphere-like morphology (Fig. 2b–d). Furthermore, as observed in Fig. 2e the size of the nanoparticles decreased to ~54 nm when the concentration of the Al dopant was 12 wt%. The results clearly confirmed that the ZnO nanorods transformed into nanoparticles upon incorporation of aluminum (Al^{3+}) in ZnO. The representative TEM images in Fig. 3a and b revealed the rod-like morphology of the undoped ZnO sample; the rods were 1.5 μm in length and 200 nm in diameter. The TEM images in Fig. 4a and b shows the irregular sphere-like morphology of AZO (6 wt% Al). The high-resolution TEM (HRTEM) images of the undoped ZnO and AZO samples revealed that the rods and nanoparticles were crystalline (Figs. 3c and 4c). The selected area electron diffraction (SAED) patterns of the ZnO nanorods (Fig. 3d) and AZO (Fig. 4d) indicated that both samples had a hexagonal structure. These results were consistent with the XRD results.

3.2. Chemical bonding and composition of AZO

Elemental analysis of AZO (6 wt% Al) was conducted by EDX and color mapping analysis. The results presented in Figs. 2f and 5a–c confirmed the existence of Zn, O, Al elements in the AZO sample. The elements were uniformly distributed in AZO sample (6 wt% Al) [28]. Fig. 6 shows the FTIR spectra of ZnO and AZO samples. The broad absorption band at 3440 cm^{-1} was ascribed to O–H bending vibration of water molecules absorbed onto the ZnO nanorods and AZO nanoparticles. The vibration at 1620 cm^{-1} was attributed to O–H vibration [29]. The peak at 684 cm^{-1} was assigned to Al–O. The sharp peak at 498 cm^{-1} was ascribed to Zn–O [30]. Fig. 7 presents the Raman scattering spectra of ZnO and AZO. The peak at 438 cm^{-1} was ascribed to the non-optical phonon E_{2H} mode, which confirmed the wurtzite structure of ZnO [31]. The weak peaks at 330 and 380 cm^{-1} were ascribed to multi-phonons scattering process E_{2H} - E_{2L} and A1 phonons, respectively. The peak at 580 cm^{-1} could be attributed to longitudinal optical E_{1L} mode [32].

3.3. Optical properties

The UV–visible absorption spectra of ZnO and AZO are shown in Fig. 8. The absorption edge values of the ZnO nanorods and AZO nanoparticles (3, 6, 9, 12 wt%) were 380, 380, 378, 377, and 375 nm, respectively. When compared with the absorption edge values of the ZnO nanorods and bulk ZnO, those of the AZO materials were blue-shifted. This phenomenon may be due to coupling effects among the particles [33].

3.4. XPS analysis

XPS analysis was conducted to analyze the distribution and oxidation state of the chemical elements in ZnO and AZO samples. Fig. 9 shows the high-resolution XPS spectra of Zn 2p, O 1s, and Al 2p of ZnO and AZO. The XPS analysis revealed that the samples consisted of C, Zn, O, and Al, and no impurities were found. Specifically, Fig. 9a shows the Zn 2p XPS pattern of the ZnO nanorods. The peaks observed at binding energies of 1023.8 and 1046.8 eV, correspond to the spin orbit of Zn $2p_{3/2}$ and Zn $2p_{1/2}$. It indicated the existence of a divalent oxidation state in the sample [34]. Al-doped ZnO showed a slight chemical shift in the binding energy compared with undoped ZnO because of the presence of Al. In Fig. 9b, the peak observed at the binding energy of 74.7 eV corresponded to Al 2p, which confirmed the successful incorporation of Al elements into Zn^{2+} sites of ZnO [35]. In Fig. 9c, the O 1s peak positioned at the lower binding energy of 530.8 eV was assigned to O^{2-} ions in the Zn–O bonding of the wurtzite structure of ZnO. In contrast, the peak located at 532.3 eV was associated with O^{-} and O^{2-} ions in oxygen-deficient regions in the sample matrix [36]. In

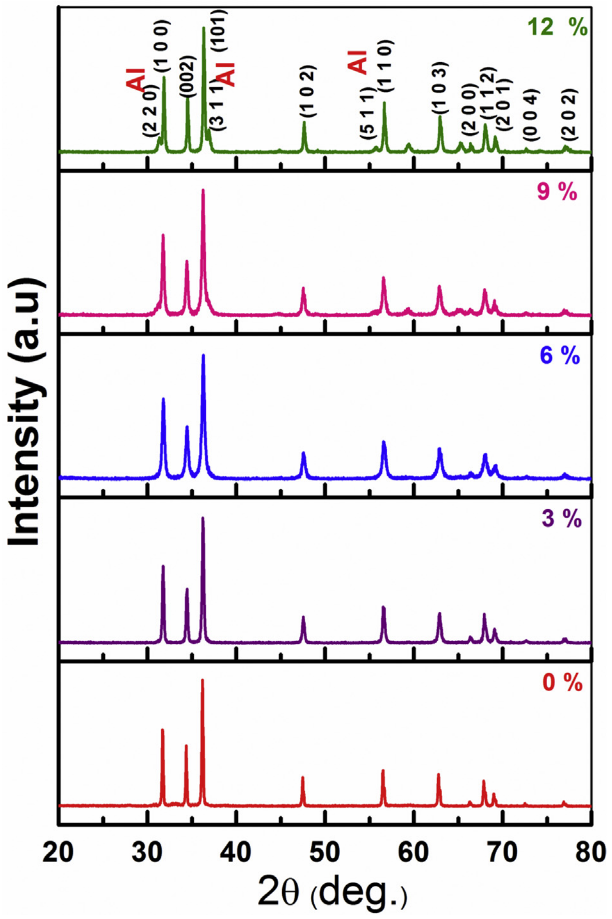

Fig. 1. X-ray diffraction (XRD) patterns of the undoped ZnO nanorods and Al-doped ZnO nanoparticles (3, 6, 9, 12 wt% Al).

Table 1
Comparison of particle size of the undoped ZnO and Al-doped ZnO.

Samples	2θ (002)	FWHM (deg)	D (nm)	a (Å)
AZO (0%)	34.3726	0.1056	78.7	4.5
AZO (3%)	34.3906	0.1674	49.6	4.5
AZO (6%)	34.4642	0.2782	29.9	5.2
AZO (9%)	34.4364	0.2374	35.0	5.8
AZO (12%)	34.4896	0.1586	52.4	5.8

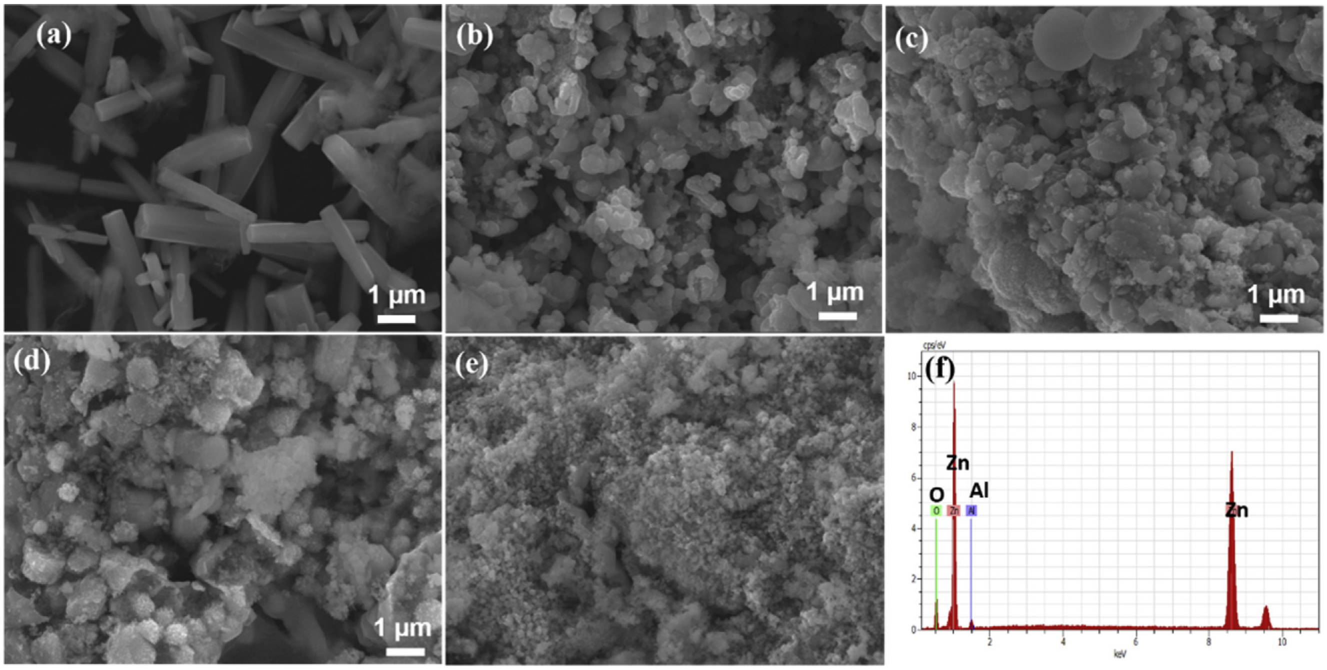

Fig. 2. Field-emission scanning electron microscopy (FESEM) images of (a) undoped ZnO, and Al-doped ZnO (AZO) at varying Al concentrations of (b) 3, (c) 6, (d) 9, and (e) 12 wt%. Energy-dispersive X-ray spectrum of AZO (6 wt%).

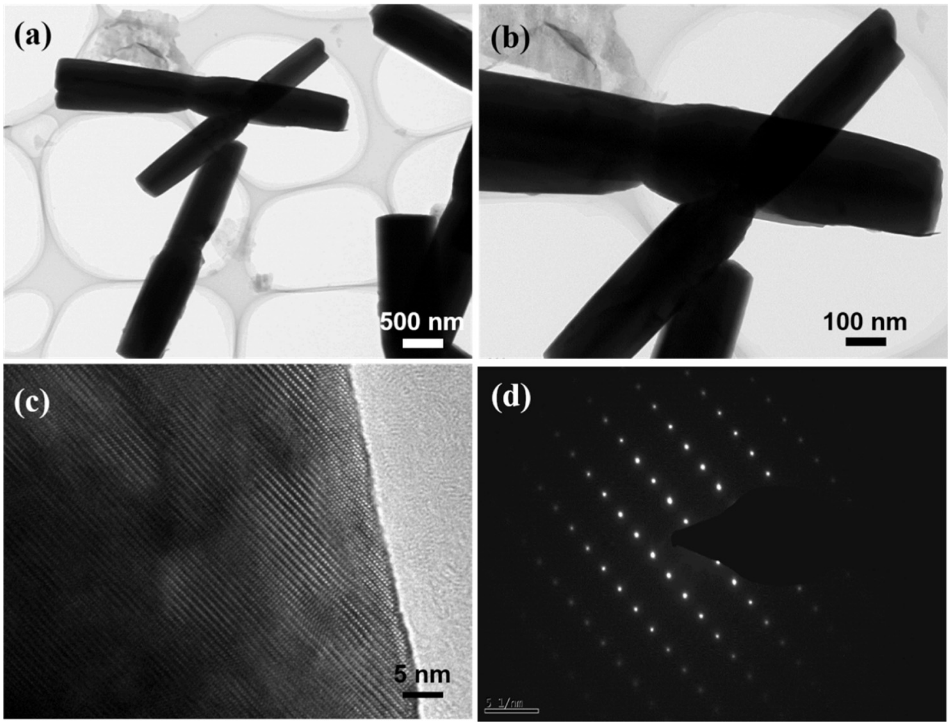

Fig. 3. (a, b) Transmission electron microscopy (TEM) images, (c) high-resolution TEM (HRTEM) images, and (d) selected area electron diffraction (SAED) pattern of the ZnO nanorods.

the pattern of the AZO sample (Fig. 9d), the peak was observed at a higher binding energy of 533.1 eV when compared with that of the ZnO nanorods. It is obvious that the AZO sample contains more O_2 species than the undoped ZnO owing to higher donor content. Hence, the surface of the AZO samples was modified because of the greater amount of oxygen vacancies [36].

3.5. N_2 adsorption and desorption analysis

N_2 adsorption–desorption analysis was conducted to further probe the surface properties of the ZnO nanorods and AZO (6 wt% Al) nanoparticles. Fig. 10a and b shows the adsorption–desorption isotherms of ZnO nanorods and AZO nanoparticles. The

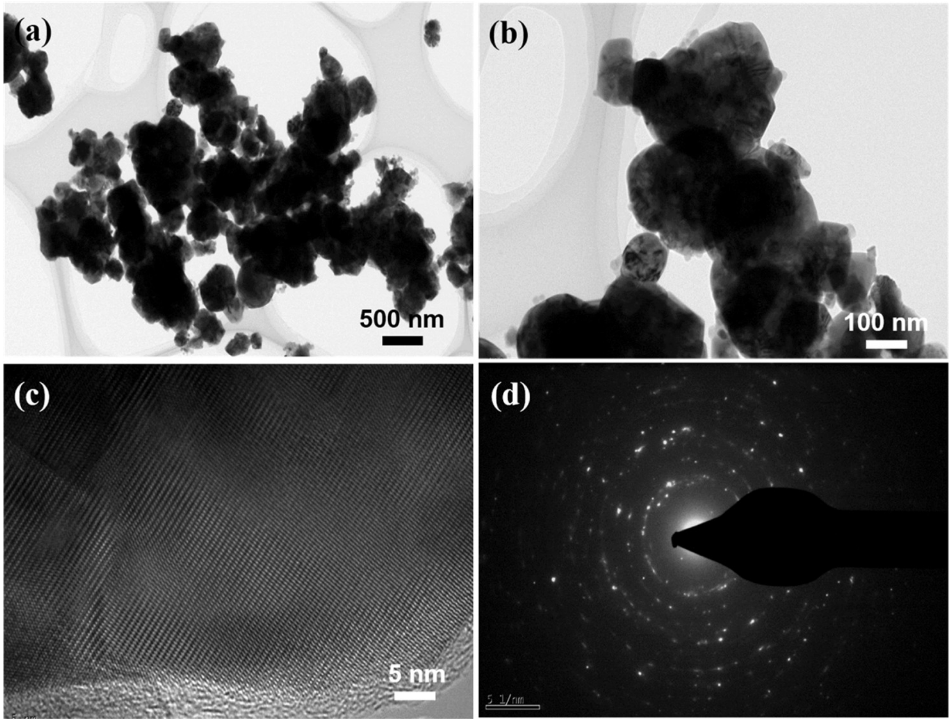

Fig. 4. (a, b) Transmission electron microscopy (TEM) images, (c) high-resolution TEM (HRTEM), and (d) selected area electron diffraction (SAED) pattern of the AZO nanoparticles.

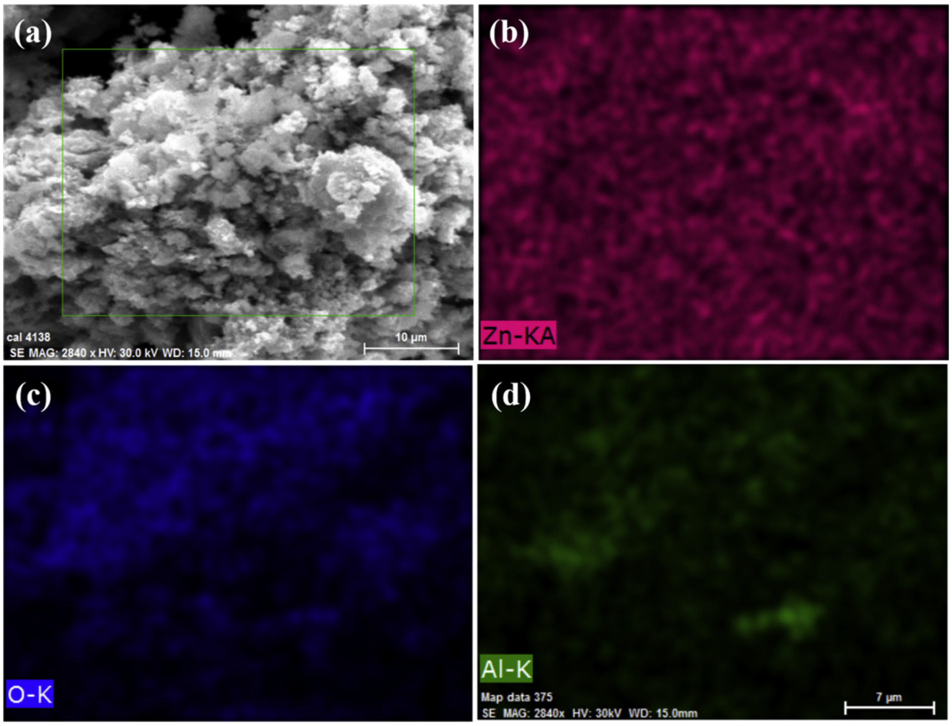

Fig. 5. Energy-dispersive X-ray spectrum and elemental color mapping of AZO (6 wt%).

Brunauer–Emmett–Teller (BET) specific surface areas of the samples were calculated from the N_2 adsorption branch. AZO nanoparticles featured a BET surface area of 404 m^2/g and the ZnO nanorods featured a BET surface area of 18 m^2/g [37]. The specific area of the AZO nanoparticles was higher than that of the undoped ZnO nanorods, since nanoparticles have high surface area than the nanorods which are consistent with the FESEM results in Fig. 2.

3.6. Gas sensing studies

3.6.1. Experimental set-up

Room temperature gas sensing studies were performed using

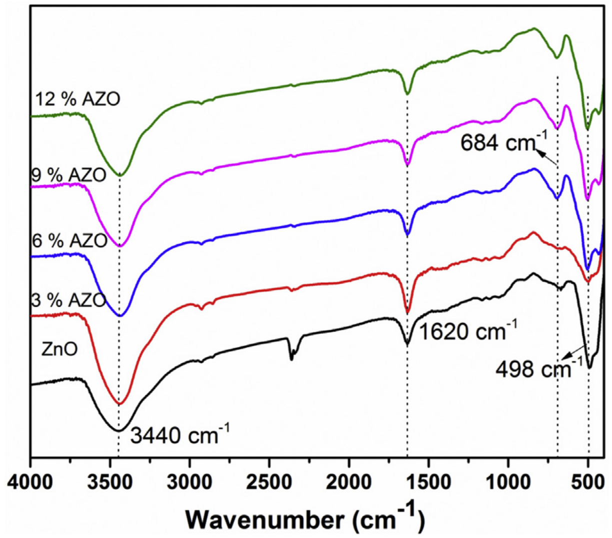

Fig. 6. Fourier transform infrared (FTIR) spectra of the undoped ZnO and Al-doped ZnO (3, 6, 9, 12 wt% Al).

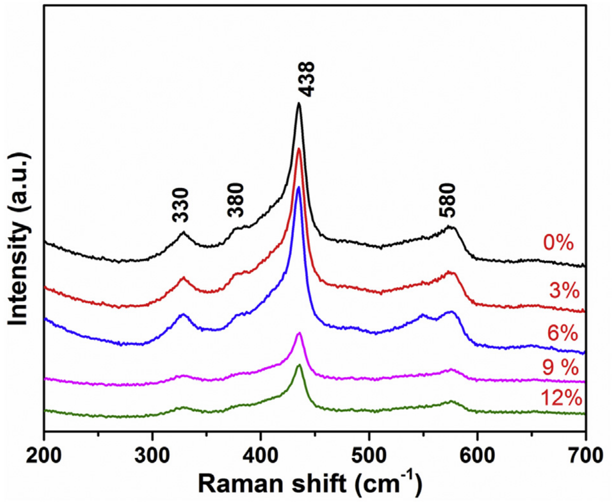

Fig. 7. Raman spectra of the undoped ZnO and Al-doped ZnO (3, 6, 9, 12 wt% Al).

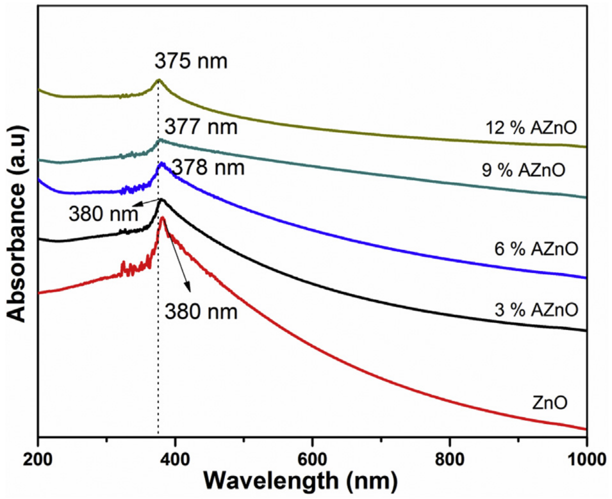

Fig. 8. UV–visible spectra of the undoped ZnO and Al-doped ZnO (3, 6, 9, 12 wt% Al).

house-built sensing setup, which was described in previous research reports [38,39]. The constant target vapor concentration (C_{ppm}) [40] inside the testing chamber was estimated using Eq. (1):

$$C_{\text{ppm}} = \frac{\delta \times V_{\text{r}} \times R \times T}{M \times P_{\text{b}} \times V_{\text{b}}} \tag{1}$$

where, δ is the density of ammonia, V_{r} is the volume of ammonia injected inside the chamber, R is the universal gas constant, T is the absolute temperature, M is the molecular weight, P_{b} is the pressure inside the chamber, and V_{b} is the volume of the chamber. The sensor response (S) was calculated [39] using Eq. (2):

$$S = \frac{R_{\text{a}}}{R_{\text{g}}} \tag{2}$$

where R_{a} and R_{g} are the resistance of the sensing element in air and target gas, respectively.

3.6.2. *Selectivity*

Selectivity is an important characteristic for evaluating the efficiency of gas sensors. Selectivity studies were therefore conducted involving various target vapors at room temperature under ambient conditions. At first, to check the effect of water vapor on ZnO films at room temperature, small amount of water was added and measured the resistance. No significant change in resistance was observed. Further, the selectivity of the undoped ZnO film towards 100 ppm of different target vapors i.e. acetone, acetaldehyde, toluene, ammonia, and ethanol was examined (Fig. 11a). The response values were 4, 7, 3, 117, and 2.5, respectively. As observed, the response value for ammonia was more than 10 times higher than those for the other target vapors. These results confirmed that the sensing element was highly selective at room temperature. There are two main reasons behind high selectivity towards ammonia. One reason may be the presence of lone pair of electrons in ammonia and high catalytic nature of the nanostructured surface. The other reason may be kinetic diameter and ionization energy of the target molecules. Lower kinetic diameter molecules may diffuse into the sensing layer quickly and hence resulted in rapid response. Ionization energy of the molecules also another reason to obtain high selectivity [38,41,42]. Even though acetone and toluene has low ionization energy than ammonia, their larger kinetic diameter will reduce the selectivity [43]. The kinetic diameter and ionization energy of various interfacing vapors are shown in Table 2.

3.6.3. *Response recovery studies*

Fig. 11b shows the response of the undoped ZnO and AZO (3, 6, 9, 12 wt% Al) thin films towards 100 ppm of ammonia gas. As observed, the response value initially increased with increasing Al concentrations then decreased with further increases in Al content before reaching a maximum value (i.e. 350) at a Al dopant level of 6 wt%.

To further evaluate the ammonia sensing properties of the prepared materials, the undoped ZnO and AZO (6 wt% Al) films were exposed to varying ammonia concentrations of 5–500 ppm (Fig. 11c). When compared with the response of the ZnO film, that of the AZO film was higher and increased as the concentration of ammonia increased. The response value of AZO (6 wt% Al) increased from 21 to 47, 78, 338, 420, and 630 as the concentration of ammonia increased from 5 to 10, 50, 100, 250, and 500 ppm. The lower response values at the lower ammonia concentrations were attributed to limited surface reaction events owing to the limited number of target molecules present for interaction. In contrast, higher concentrations of ammonia resulted in more and

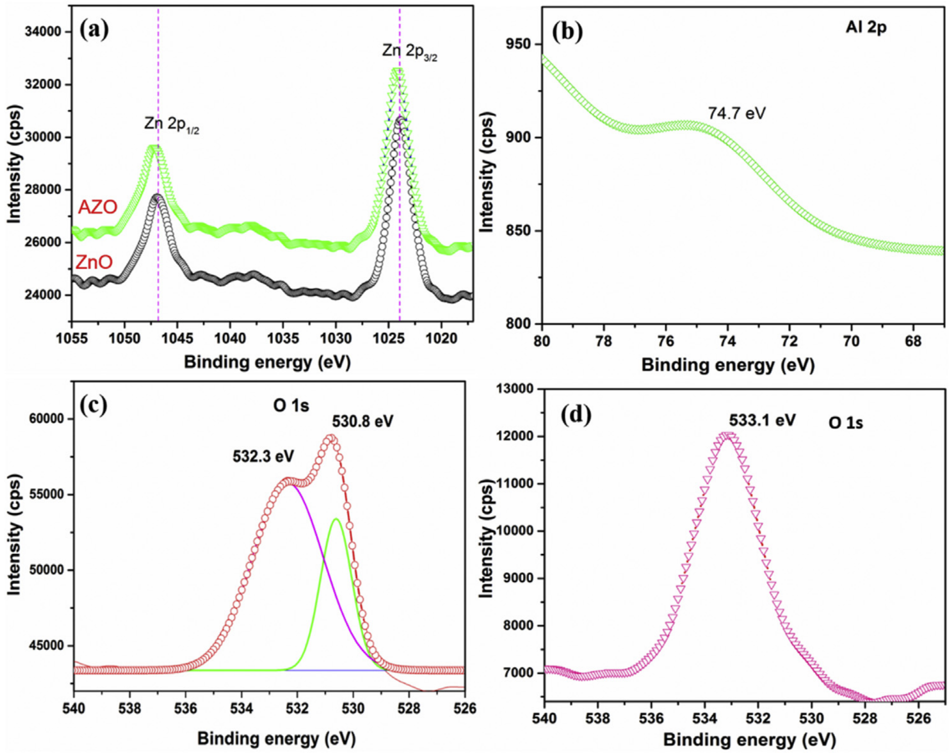

Fig. 9. X-ray photoelectron spectroscopy (XPS) analysis of the undoped ZnO and Al-doped ZnO: (a) Zn 2p XPS pattern of ZnO nanorods; (b) Al 2p XPS pattern of Al-doped ZnO (6 wt %); (c) O 1s XPS pattern of ZnO nanorods, and (d) O 1s XPS pattern of Al-doped ZnO (6 wt%).

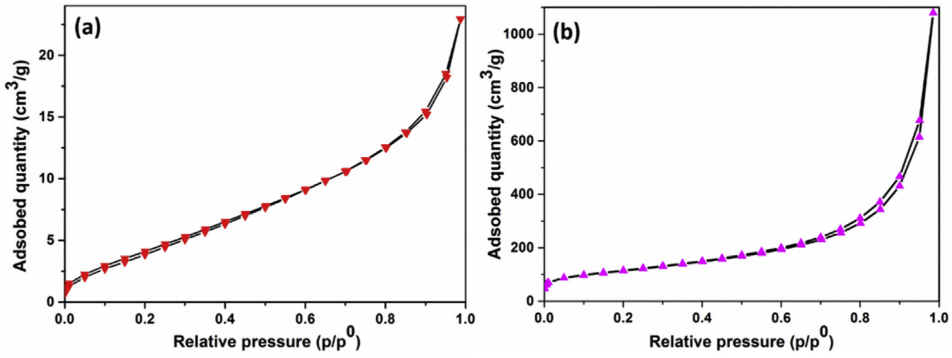

Fig. 10. N_2 adsorption–desorption isotherms of the ZnO nanorods and AZO nanoparticles.

simultaneous interaction events, which led to increase in the response. The transient resistance response curves of ZnO and AZO (6 wt% Al) thin films are shown in Fig. 11d. The transient plots clearly show the rise and fall behaviors of resistance in the presence and absence of ammonia. The transient response plots indicated that the sensing response was governed by the reaction between ammonia and chemisorbed oxygen species. The observed sensitivity was found to be significant compared with other doped ZnO material (see Table 3).

3.6.4. Sensing mechanism

Metal oxide sensing mechanism is mainly manifested by changes in the height of the potential barrier between grains and grain barriers during gas–solid interactions. During gas–solid interactions, several events occur on the grains such as the adsorption of oxygen species on the grains surface, redox reactions between the grains and gases, electron transfer among the grains, and desorption of the target gas from the grains [49,50]. Gas sensing begins with the adsorption of oxygen species. The oxygen from the atmosphere is adsorbed onto the surface of the sensor by trapping an electron and is chemisorbed in the form of O_2^-, O^-, and O^{2-} depending on the sensor operating temperature. At room temperature, the chemisorbed oxygen state [51] varies as follows:

$$O_{2(gas)} + e^- \leftrightarrow O^-_{2(ads)} \tag{3}$$

$$O^-_{2(ads)} + e^- \leftrightarrow O^-_{(lattice)} \tag{4}$$

The chemisorbed oxygen species captures an electron from the conduction band of the sensing material, resulting in an increase in the resistance of the n-type sensing material until equilibrium is attained with the ambient oxygen atmosphere (baseline resistance). When the NH_3 gas interacts with the chemisorbed oxygen species, it readily oxidizes to N_2, H_2O, and an electron [36]. These

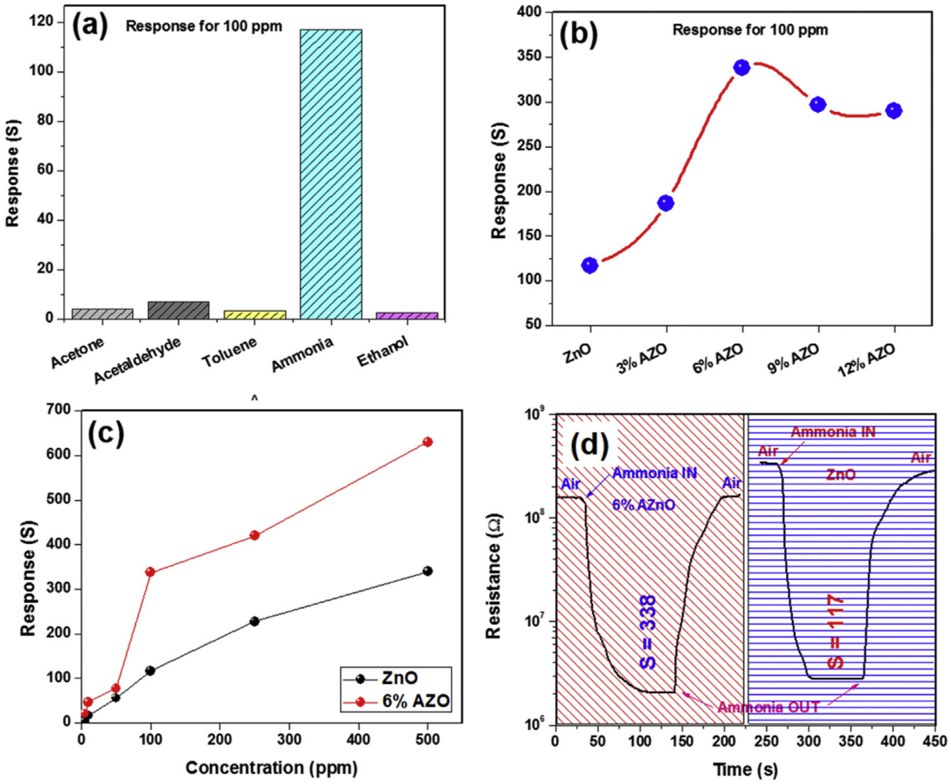

Fig. 11. (a) Selectivity of the ZnO thin films exposed to 100 ppm of various target gases. (b) Sensing response of the pure ZnO and AZO thin films exposed to 100 ppm of ammonia. (c) Response of the undoped ZnO and AZO (6 wt%) thin films exposed to varying concentrations of ammonia. (d) Transient resistance response plots of the undoped ZnO and AZO (6 wt%) films towards 100 ppm of ammonia.

Table 2
Kinetic diameter and ionization energy of various interfering vapors.

Vapor	Kinetic diameter (nm)	Ionization energy (eV)
Acetone	0.46	9.69
Acetaldehyde	0.39	10.21
Toluene	0.58	8.82
Ammonia	0.36	10.18
Ethanol	0.45	10.47

electrons are released into the conduction band of the metal oxide, resulting in a decrease in the resistance of the sensor material. The interaction between the chemisorbed oxygen species and ammonia can be described as follows:

$$4NH_3 + 3O_{2(ads)}^{-} \leftrightarrow 2N_2 + 6H_2O + 3e^{-} \quad (5)$$

The defect states and oxygen vacancies play important roles in tuning the electrical properties of metal oxides. From the thermodynamics point of view, point defects are the inherent part of ZnO, resulting in the non-stoichiometric nature. In the case of AZO, the substitution of Zn^{2+} with Al^{3+} is largely effective because of the large ionic size difference between Al^{3+} and Zn^{2+} ions. The ionic radius of Al^{3+} (0.057 nm) is smaller than that of Zn^{2+} (0.074 nm). However, the positive valence charge resulting from substitution needs to be compensated by the release of an extra electron to maintain charge neutrality. The released free electrons are introduced into the conduction band of ZnO, thus increasing the electron concentration, which leads to a slight upward shift of the Fermi level to the conduction band. The Kröger–Vink notation is described as follows:

$$Al_2O_3 \rightarrow 2Al_{Zn} + 3O_0^{x} + 2e^{-} \quad (6)$$

where Al_{Zn} is the Al ion substitution in the Zn lattice with positive charge and $O^{x}{}_{0}$ refers to the oxygen ion in the oxygen lattice with neutral charge [52]. Hence, Al doping in ZnO produces point defects and more oxygen vacancies, which are beneficial towards

Table 3
Comparison of room temperature NH_3 sensing characteristics of ZnO based sensors reported so far and current work.

Material	Structure	Concentration (ppm)	Response (S)	Refs.
$ZnO + Cr_2O_3$	Thick film	300	13.7	[44]
ZnO + camphor + PANI	Nanocomposite	100	28	[45]
ZnO + Ni	Thin film	100	105	[46]
ZnO	Thin film	25	233	[39]
ZnO + Co	Thin film	100	3.48	[40]
ZnO + Ni	Thin film	100	2.52	[42]
ZnO + Cd	Thin film	100	5	[47]
ZnO nanorod	Thin film	100	22.8	[48]
ZnO + Al	Thin film	100	350	This work

improving the gas sensing performance. Above a certain doping concentration, the film conductivity becomes very high, and during gas–solid interactions, the change in the potential barrier height is minimal, thereby resulting in poor gas sensing performance.

4. Conclusion

ZnO nanorods and Al-doped ZnO nanoparticles were successfully synthesized by sol–gel method. FESEM analysis revealed the transformation of the nanorods into sphere-like particles upon incorporation of Al in the ZnO nanorods. Al-doped ZnO (6 wt%) nanoparticles showed a rapid response of 350 when compared with undoped ZnO. Furthermore, the response of the Al-doped ZnO (6 wt%) nanoparticles increased with increasing ammonia concentrations from 5 to 500 ppm. The high response displayed by Al-doped ZnO (6 wt%) towards NH_3 can be attributed to the presence of numerous oxygen vacancies, which promotes oxygen adsorption. The large amount of oxygen absorbed on the surface of the Al-doped ZnO surface enhanced the oxidizing potential of NH_3

Acknowledgements

R. sankar ganesh thanks MEXT-Japan for award of a research fellowship. The authors thank the Center for Instrumental Analysis, Shizuoka University, Hamamatsu, Japan, and the Department of Physics and Nanotechnology, SRM University, Kattankulathur, India, at which the characterization analyses were conducted.

References

[1] T. Seiyama, K. Fujiishi, M. Nagatani, A. Kato, A new detector for gaseous components using zinc oxide thin films, J. Soc. Chem. Ind. Jpn. 66 (1963) 652–655.

[2] T. Seiyama, S. Kagawa, Study on a detector for gaseous components using semiconductive thin films, Anal. Chem. 38 (1966) 1069–1073.

[3] I.D. Kim, A. Rothschild, T. Hyodo, H.L. Tuller, Microsphere templating as means of enhancing surface activity and gas sensitivity of $CaCu_3Ti_4O_{12}$ thin films, Nano Lett. 6 (2006) 193–198.

[4] C.W. Na, H.-S. Woo, I.-D. Kim, J.-H. Lee, Selective detection of NO_2 and C_2H_5OH using a Co_3O_4-decorated ZnO nanowire network sensor, Chem. Commun. Camb. 47 (2011) 5148–5150.

[5] L. Liao, H.B. Lu, J.C. Li, H. He, D.F. Wang, D.J. Fu, C.L.F. Zhang, C. Liu, Size Dependence of Gas Sensitivity of ZnO Nanorods Size Dependence of Gas Sensitivity of ZnO Nanorods, vol. 111, 2007, pp. 1900–1903.

[6] F. Paraguay, D.M. Miki-Yoshida, J. Morales, J. Solis, W. Estrada, Influence of Al, In, Cu, Fe and Sn dopants on the response of thin film ZnO gas sensor to ethanol vapour, Thin Solid Films 373 (2000) 137–140.

[7] P.P. Sahay, R.K. Nath, Al-doped zinc oxide thin films for liquid petroleum gas (LPG) sensors, Sensors Actuators B Chem. 133 (2008) 222–227.

[8] G.N. Narayanan, R.S. Ganesh, A. Karthigeyan, Effect of annealing temperature on structural, optical and electrical properties of hydrothermal assisted zinc oxide nanorods, Thin Solid Films 598 (2016) 39–45.

[9] S.S. Badadhe, I.S. Mulla, H_2S gas sensitive indium-doped ZnO thin films: preparation and characterization, Sensors Actuat. B Chem. 143 (2009) 164–170.

[10] H. Gong, J.Q. Hu, J.H. Wang, C.H. Ong, F.R. Zhu, Nano-crystalline Cu-doped ZnO thin film gas sensor for CO, Sensors Actuat. B Chem. 115 (2006) 247–251.

[11] W. Cao, Y. Duan, Optical fiber-based evanescent ammonia sensor, Sensors Actuat. B Chem. 110 (2005) 252–259.

[12] M. Yin, F. Wang, H. Fan, L. Xu, S. Liu, Heterojunction CuO@ZnO microcubes for superior p-type gas sensor application, J. Alloys Compd. 672 (2016) 374–379.

[13] M. Hjiri, L. El Mir, S.G. Leonardi, A. Pistone, L. Mavilia, G. Neri, Al-doped ZnO for highly sensitive CO gas sensors, Sensors Actuat. B Chem. 196 (2014) 413–420.

[14] P.P. Sahay, R.K. Nath, Al-doped ZnO thin films as methanol sensors, Sensors Actuat. B Chem. 134 (2008) 654–659.

[15] X. Liu, K. Pan, W. Li, D. Hu, S. Liu, Y. Wang, Optical and gas sensing properties of Al-doped ZnO transparent conducting films prepared by sol-gel method under different heat treatments, Ceram. Int. 40 (2014) 9931–9939.

[16] S.C. Vattappalam, D. Thomas, S. Augustine, S. Mathew, Effect of electron irradiation on gas sensing properties of Al-Zno, Cogent. Phys. 2 (2015) 1019664.

[17] R. Yoo, S. Cho, M.J. Song, W. Lee, Highly sensitive gas sensor based on Al-doped ZnO nanoparticles for detection of dimethyl methylphosphonate as a chemical warfare agent simulant, Sensors Actuat. B Chem. 221 (2015) 217–223.

[18] W.W. Zhong, F.M. Liu, L.G. Cai, Peng-Ding, C.C. Zhou, L.G. Zeng, X.Q. Liu, Y. Li, Elaboration and characterization of Al doped ZnO nanorod thin films annealed in hydrogen, J. Alloys Compd. 509 (2011) 3847–3851.

[19] A. Patil, C. Dighavkar, R. Borse, Al Doped ZnO Thick Films as CO_2 Gas Sensors, vol. 13, 2011, pp. 1331–1337.

[20] Y.S. Kim, W.P. Tai, Electrical and optical properties of Al-doped ZnO thin films by sol-gel process, Appl. Surf. Sci. 253 (2007) 4911–4916.

[21] M. Behrens, G. Lolli, N. Muratova, I. Kasatkin, M. Hävecker, R.N. D'Alnoncourt, O. Storcheva, K. Köhler, M. Muhler, R. Schlögl, The effect of Al-doping on ZnO nanoparticles applied as catalyst support, Phys. Chem. Chem. Phys. 15 (2013) 1374–1381.

[22] D. Gautam, M. Engenhorst, C. Schilling, G. Schierning, R. Schmechel, M. Winterer, Thermoelectric properties of pulsed current sintered nanocrystalline Al-doped ZnO by chemical vapour synthesis, J. Mater. Chem. A 3 (2015) 189–197.

[23] I. Rawal, Facial synthesis of hexagonal metal oxide nanoparticles for low temperature ammonia gas sensing applications, RSC Adv. 5 (2015) 4135–4142, http://dx.doi.org/10.1039/C4RA12747A.

[24] C.S. Rout, M. Hegde, A. Govindaraj, C.N.R. Rao, Ammonia sensors based on metal oxide nanostructures, Nanotechnology 18 (2007) 205504, http://dx.doi.org/10.1088/0957-4484/18/20/205504.

[25] K.H. Kim, T. Umakoshi, Y. Abe, M. Kawamura, T. Kiba, Morphological properties of Al-doped ZnO nano/microstructures, Superlattices Microstruct. 91 (2016) 188–192.

[26] A. Nakrela, N. Benramdane, A. Bouzidi, Z. Kebbab, M. Medles, C. Mathieu, Results in Physics Site location of Al-dopant in ZnO lattice by exploiting the structural and optical characterisation of ZnO: Al thin films, Results Phys. 6 (2016) 133–138.

[27] A. Alkahlout, N. Al Dahoudi, I. Grobelsek, M. Jilavi, P.W. De Oliveira, Synthesis and characterization of aluminum doped zinc oxide nanostructures via hydrothermal route, J. Mater 2014 (2014) 8.

[28] A. Vanaja, G.V. Ramaraju, S. Rao, Structural and optical investigation of Al doped ZnO nanoparticles synthesized by sol-gel process, Indian J. Sci. Technol. 9 (2016) 87013–87019.

[29] A.N. Mallika, A. Ramachandrareddy, K. Sowribabu, K. Venugopal Reddy, Synthesis and optical characterization of aluminum doped ZnO nanoparticles, Ceram. Int. 40 (2014) 12171–12177.

[30] N.R. Yogamalar, A. Chandra Bose, Absorption-emission study of hydrothermally grown Al:ZnO nanostructures, J. Alloys Compd. 509 (2011) 8493–8500.

[31] J.C. Sin, S.M. Lam, K.T. Lee, A.R. Mohamed, Self-assembly fabrication of ZnO hierarchical micro/nanospheres for enhanced photocatalytic degradation of endocrine-disrupting chemicals, Mater. Sci. Semicond. Process 16 (2013) 1542–1550.

[32] J. Zhao, L. Wang, X. Yan, Y. Yang, Y. Lei, J. Zhou, Y. Huang, Y. Gu, Y. Zhang, Structure and photocatalytic activity of Ni-doped ZnO nanorods, Mater. Res. Bull. 46 (2011) 1207–1210.

[33] M. Ramani, S. Ponnusamy, C. Muthamizhchelvan, J. Cullen, S. Krishnamurthy, E. Marsili, Morphology-directed synthesis of ZnO nanostructures and their antibacterial activity, Colloids Surfaces B Biointerfaces 105 (2013) 24–30.

[34] J.T. Chen, J. Wang, R.F. Zhuo, D. Yan, J.J. Feng, F. Zhang, P.X. Yan, The effect of Al doping on the morphology and optical property of ZnO nanostructures prepared by hydrothermal process, Appl. Surf. Sci. 255 (2009) 3959–3964.

[35] J. Wang, Y. Li, Y. Kong, J. Zhou, J. Wu, X. Wu, W. Qin, Z. Jiao, L. Jiang, Non-fluorinated superhydrophobic and micro/nano hierarchical Al doped ZnO film: the effect of Al doping on morphological and hydrophobic properties, RSC Adv. 5 (2015) 81024–81029.

[36] S. Bai, T. Guo, Y. Zhao, R. Luo, D. Li, A. Chen, C.C. Liu, Mechanism enhancing gas sensing and first-principle calculations of Al-doped ZnO nanostructures, J. Mater. Chem. A 1 (2013) 11335–11342.

[37] Y.C. Chen, L.H. Chen, Y.L. Min, Y.G. Zhang, Simple method to synthesize novel mesoporous zinc oxide, J. Mater. Sci. Mater. Electron. 23 (2012) 1759–1763.

[38] G.K. Mani, J.B.B. Rayappan, Novel and facile synthesis of randomly interconnected ZnO nanoplatelets using spray pyrolysis and their room temperature sensing characteristics, Sensors Actuat. B Chem. 198 (2014) 125–133.

[39] G.K. Mani, J.B.B. Rayappan, A highly selective room temperature ammonia sensor using spray deposited zinc oxide thin film, Sensors Actuat. B Chem. 183 (2013) 459–466.

[40] G.K. Mani, J.B.B. Rayappan, A highly selective and wide range ammonia sensor – nanostructured ZnO: Co thin film, Mater. Sci. Eng. B Solid-State Mater. Adv. Technol. 191 (2015) 41–50.

[41] A.J. Kulandaisamy, J.R. Reddy, P. Srinivasan, K.J. Babu, G.K. Mani, P. Shankar, J.B.B. Rayappan, Room temperature ammonia sensing properties of ZnO thin films grown by spray pyrolysis: effect of Mg doping, J. Alloys Compd. 688 (2016) 422–429.

[42] G.K. Mani, J.B.B. Rayappan, Selective detection of ammonia using spray pyrolysis deposited pure and nickel doped ZnO thin films, Appl. Surf. Sci. 311 (2014) 405–412.

[43] P. Shankar, J. Bosco, B. Rayappan, Gas sensing mechanism of metal oxides: the role of ambient atmosphere, type of semiconductor and gases – a review, Sci. Jet. 4 (2015) 126.

[44] D.R. Patil, L.A. Patil, P.P. Patil, Cr_2O_3 -activated ZnO thick film resistors for ammonia gas sensing operable at room temperature, Sensors Actuat. B 126 (2007) 368–374.

[45] S.L. Patil, M.A. Chougule, S. Sen, V.B. Patil, Measurements on room

temperature gas sensing properties of CSA doped polyaniline – ZnO nanocomposites, Measurement 45 (2012) 243–249.
[46] O.I. Lupan, S.T. Shishiyanu, T.S. Shishiyanu, Nitrogen Oxides and Ammonia Sensing Characteristics of SILAR Deposited ZnO Thin Film, vol. 42, 2007, pp. 375–378.
[47] N.L. Tarwal, A.R. Patil, N.S. Harale, A.V. Rajgure, S.S. Suryavanshi, W.R. Bae, P.S. Patil, J.H. Kim, J.H. Jang, Gas sensing performance of the spray deposited Cd-ZnO thin films, J. Alloys Compd. 598 (2014) 282–288.
[48] S. Anantachaisilp, S.M. Smith, C. Ton-that, T. Osotchan, A.R. Moon, M.R. Phillips, Tailoring deep level surface defects in ZnO nanorods for high sensitivity ammonia gas sensing, J. Phys. Chem. C 118 (2014) 27150–27156.
[49] Y.-F. Sun, S.-B. Liu, F.-L. Meng, J.-Y. Liu, Z. Jin, L.-T. Kong, J.-H. Liu, Metal oxide nanostructures and their gas sensing properties: a Review, Sensors 12 (2012) 2610–2631.
[50] G.K. Mani, J.B.B. Rayappan, ZnO nanoarchitectures: ultrahigh sensitive room temperature acetaldehyde sensor, Sensors Actuat. B Chem. 223 (2016) 343–351.
[51] J.R. Reddy, G.K. Mani, P. Shankar, J.B.B. Rayappan, Spray pyrolysis deposited zno nanopebbles as room temperature ammonia sensor, Sens. Lett. 12 (2014) 1451–1456.
[52] S. Mondal, S. Bhattacharya, P. Mitra, Structural, morphological, and lpg sensing properties of al-doped zno thin film prepared by SILAR, Adv. Mater. Sci. Eng. 2013 (2013) 1–6.